IEEE Access
Multidisciplinary | Rapid Review | Open Access Journal

Received January 13, 2018, accepted February 13, 2018, date of publication February 27, 2018, date of current version April 4, 2018.

Digital Object Identifier 10.1109/ACCESS.2018.2810085

Wideband Fabry-Perot Resonator Antenna With Electrically Thin Dielectric Superstrates

NAIZHI WANG[1], LARBI TALBI[2], (Senior Member, IEEE), QINGSHENG ZENG[3], (Senior Member, IEEE), AND JIADONG XU[4]

[1]The 14th Research Institute of China Electronics Technology Group Corporation, Nanjing 210039, China
[2]Department of Computer Science and Engineering, University of Quebec in Outaouais, Gatineau, QC J8Y 3G5, Canada
[3]College of Astronautics, Nanjing University of Aeronautics and Astronautics, Nanjing 210016, China
[4]School of Electronics and Information, Northwestern Polytechnical University, Xi'an 710072, China

Corresponding author: Naizhi Wang (naizhiwang@hotmail.com)

This work was supported by the Natural Sciences and Engineering Research Council of Canada.

ABSTRACT This paper presents a design method of wideband Fabry–Perot resonator antennas (FPRAs) with two layers of electrically thin dielectric superstrates. The bandwidth enhancement mainly benefits from the superstrate structure with reflection phase increasing with frequency, which is used as a partially reflective surface. The proposed method is validated by a design example in *X*-band. Experimental results of the FPRA prototype demonstrate that the 3-dB gain bandwidth ranges from 8.5 to 11.2 GHz (relatively 28%) with a peak gain of 14 dBi and coincides with the impedance band for $S_{11} \leqslant -10$ dB. Compared with the existing methods of gain bandwidth enhancement, the one presented in this paper does not need dielectric substrates with a large or fixed electrical thickness, improving cost performance and design flexibility.

INDEX TERMS Fabry-Perot resonator antennas, full-dielectric superstrate, high gain, wide band.

I. INTRODUCTION

Fabry-Perot resonator antennas (FPRAs) fall under the category of high-gain antennas and have received great interest from antenna community due to their compact profile, fabrication simplicity and cost-saving potential when compared with bulky horns or corporate-fed arrays [1]. Typically, FPRAs are formed by placing a primary radiator, such as a printed patch or a waveguide aperture, in a cavity between a partially reflective surface (PRS) and a metal ground plane [2], as shown in Fig. 1. The resonance of the cavity results in a cophasal and tapered field distribution along the lateral direction, and further produces high directivity with low sidelobes. FPRAs with various features have been reported in the literature, including low-profile [3], circularly polarized [4], multi-band [5], wideband [6] and beam scannable [7].

According to the ray-tracing analysis in [8], the resonance condition of the cavity can be formulated as

$$f_0 = \frac{c}{4\pi h}\left(\varphi_{PRS} + \varphi_{GND} - 2N\pi\right), \quad N = 0, 1, 2, \ldots \quad (1)$$

where f_0 is the resonance frequency; h is the depth of the cavity; φ_{PRS} and φ_{GND} are the reflection phases of the PRS and the ground plane, respectively. Due to that h and φ_{PRS} are frequency-sensitive, conventional FPRAs only possess a small gain bandwidth. Besides, the bandwidth will further reduce while the gain increases. For example, for a gain of 15 dBi, the 3 dB gain bandwidth of FPRAs is around 13%, and for 20 dBi, only 6% is available [9]. With $\varphi_{GND} = \pi$, the formulation demonstrates that if reflection phase of the PRS φ_{PRS} increases with resonance frequency f_0 (namely, with a positive slope versus frequency), FPRAs will produce a wideband resonance accompanied by an enhanced gain bandwidth. This kind of PRS is reported in [6] and [10] and has been successfully applied to wideband FPRA designs. They are either constructed with double-layered printed frequency selective surfaces (FSSs) or double-layered full-dielectric superstrates, and have the gain bandwidth of FPRAs all nearly doubled.

Using dielectric substrates to form PRSs with positive reflection phase slopes have been proposed by far in [8], [10], and [11]. In [8] and [11], a double-layered dielectric superstrate structure to enhance the gain bandwidth of FPRAs is proposed, which is composed of two substrate layers with the same permittivity and thickness of $\lambda_d/2$ and $\lambda_d/4$ (where λ_d is the dielectric wavelength at f_0), respectively. In [10],

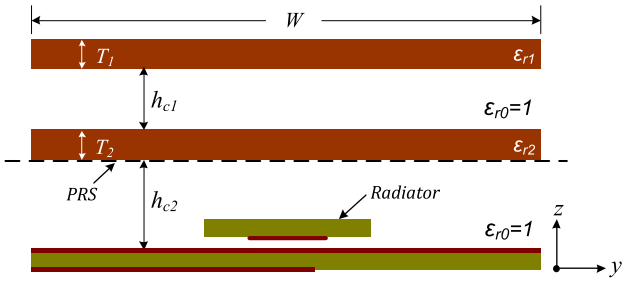

FIGURE 1. General configuration of the FPRA.

a double-layered superstrate is constructed using two substrate layers with different permittivities but with the same thickness of $\lambda_d/4$. To some extent, it reduces the dependence on thick dielectric substrates. However, $\lambda_d/4$ -thick dielectric substrates at a specific frequency are still not reachable, which increases the application cost or decreases the design flexibility in most circumstances.

In this paper, a double-layered superstrate design is presented, which is composed of two electrically thin substrate layers with the same or different permittivities. The reflection phase of the superstrate structure φ_{PRS} increases with frequency and the phase curve slope approximately satisfies the relationship of equation (1). A wideband FPRA working in X band is designed with the proposed superstrate structure, whereafter experiments are carried out for validation. This work is an improvement of the one presented in [10]. The thickness of each superstrate layer can be less than $\lambda_d/4$ and is no longer limited to a fixed value, making corresponding FPRA designs cost-effective and flexible.

II. SUPERSTRATE DESIGN

Firstly, review the superstrate structure we proposed in [10], as shown in Fig. 2a. It is composed of two dielectric substrates spaced by an air gap with thickness $h_{c1} = \lambda_0/2$. They have different permittivities ε_{r1} and ε_{r2}, where $\varepsilon_{r2} > \varepsilon_{r1}$, but the same electrical thickness $T = \lambda_d/4$. The structure can be equated with three cascaded transmission line segments, as shown in Fig. 2b. They are with characteristic impedance $Z_1 = Z_{air}/\sqrt{\varepsilon}_{r1}$, Z_{air} and $Z_2 = Z_{air}/\sqrt{\varepsilon}_{r2}$, respectively, where Z_{air} is the wave impedance of air. Moreover, the semi-infinite free space above the structure is modeled as a broadband load with impedance Z_{air}, while that beneath the structure is envisioned as a transmitter U_g with output impedance $Z_g = Z_{air}$. Hence, the reflection coefficient at the observation position Γ_3 is equivalent to that of the PRS structure.

For a physical insight, analysis of the equivalent circuit from $(f_0 - \delta f)$ to $(f_0 + \delta f)$ is carried out on the Smith Chart normalized to Z_{air}, as shown in Fig. 2c. Γ_0 is a point at the matching center and frequency-independent. Curve 1, 2 and 3 denote the loci of the reflection coefficient Γ_1, Γ_2 and Γ_3 on Smith Chart, respectively. The swirled part of the impedance curve of Γ_3 produces a positive reflection phase slope in the vicinity of f_0. According to the transmission line theory,

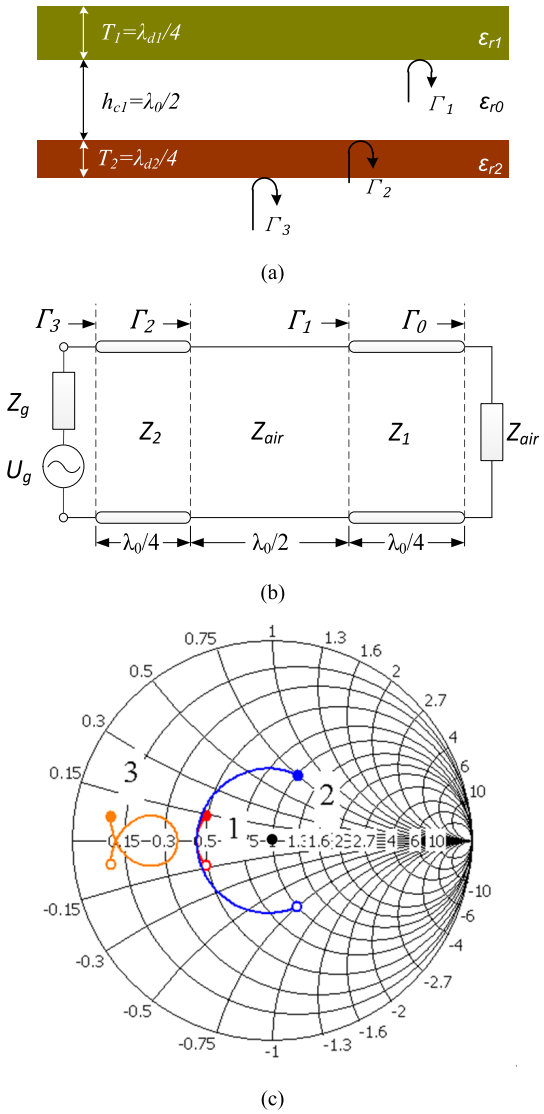

FIGURE 2. Equivalent circuit analysis: (a) superstrate structure, (b) equivalent circuit, and (c) analysis on Smith Chart normalized to Z_{air} (○: $f_r - \delta f$, ●: $f_r + \delta f$).

the magnitude of Γ_3 at f_0 can be formulated as

$$|\Gamma_3| = \left| \frac{\varepsilon_{r2} - \varepsilon_{r1}}{\varepsilon_{r2} + \varepsilon_{r1}} \right| \tag{2}$$

$|\Gamma_3|$ is proportional to $\varepsilon_{r2}/\varepsilon_{r1}$. Concluded from a set of simulations, along with $\varepsilon_{r2}/\varepsilon_{r1}$ increasing, the frequency band where the reflection phase slope is positive becomes narrower. In other words, a larger value of $\varepsilon_{r2}/\varepsilon_{r1}$ can produce a higher gain, but will diminish the gain bandwidth of the FPRA.

Dielectric substrates of Rogers RT/duroid 5880 ($\varepsilon_{r1} = 2.2$) with thickness $T_1 = 3.175$ mm and Rogers RT/duroid 6006 ($\varepsilon_{r2} = 6.15$) with thickness $T_2 = 1.9$ mm are selected to construct the superstrate structure. Their thicknesses are both $\lambda_d/4$ at 16GHz. Fig. 3 plots the reflection phase and magnitude of the structure. And with the structure, a wideband

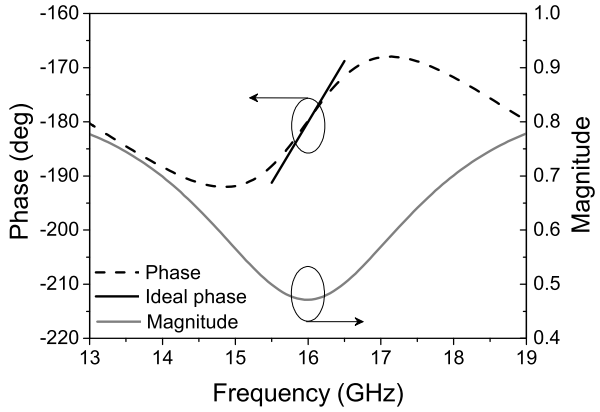

FIGURE 3. Reflection phase and magnitude of the superstrate structure.

FPRA is realized, achieving a 3 dB gain bandwidth from 13.5 GHz to 17.5 GHz, relatively 25.8%, and a peak gain of 15 dBi [10].

The bandwidth enhancement approach depicted above results in an evident improvement in gain bandwidth, but two deficiencies restrain the extension to further applications. One is that the two dielectric substrates used to construct the superstrate structure must have different permittivities. The other is that electrically thick substrates are needed and each thickness is nearly a fixed value once the desired frequency is specified. In practical designs, it is not easy to find dielectric substrates meeting the requirements from commercial products. Hence, we propose the following approach to make up the above deficiencies.

Consider the superstrate structure shown in Fig. 4a, which is similar to that in Fig. 2a but with $T_1 < \lambda_d/4$, $T_2 < \lambda_d/4$ and $\varepsilon_{r2} > \varepsilon_{r1}$. It is modeled as the equivalent circuit shown in Fig. 4b. Fig. 4c and Fig. 4d plot the loci of $\Gamma_1, \Gamma_2, \Gamma_3$ and Γ_4 on Smith Chart as Curve 1, 2, 3 and 4, respectively. Due to impedance transformation of transmission line Z_1, Γ_0 travels clockwise producing Curve 1 which represents Γ_1 within $(f_0-\delta f, f_0+\delta f)$. It can be observed that Γ_0 does not travel far enough to have the center point f_0 of Γ_1 reach the real axis of Smith Chart because $T_1 < \lambda_d/4$. For compensation, an extra air layer with thickness T_c is added, as shown in Fig. 4a, and T_c is formulated as

$$T_c = \frac{(\varphi_1 - \pi)\cdot\lambda_0}{4\pi} \tag{3}$$

where φ_1 is the reflection phase of Γ_1 at f_0 and $\pi \le \varphi_1 \le 2\pi$ due to $T_1 < \lambda_d/4$; λ_0 is the free space wavelength at f_0. Under the action of the air layer T_c, Curve 1 is turned into Curve 2 intersecting the real axis of Smith Chart at the center frequency f_0. The air layer with thickness $\lambda_0/2$ brings no change to the magnitude of Γ_2 but further spreads the curve versus frequency to Curve 3 because travel distances of impedance points on Smith Chart are proportional to frequency. Regarding the bottom dielectric superstrate, its characteristic impedance has the relationship of $Z_2 < Z_1$ because $\varepsilon_{r2} > \varepsilon_{r1}$. It swirls Curve 3 and turns it into Curve 4 as shown

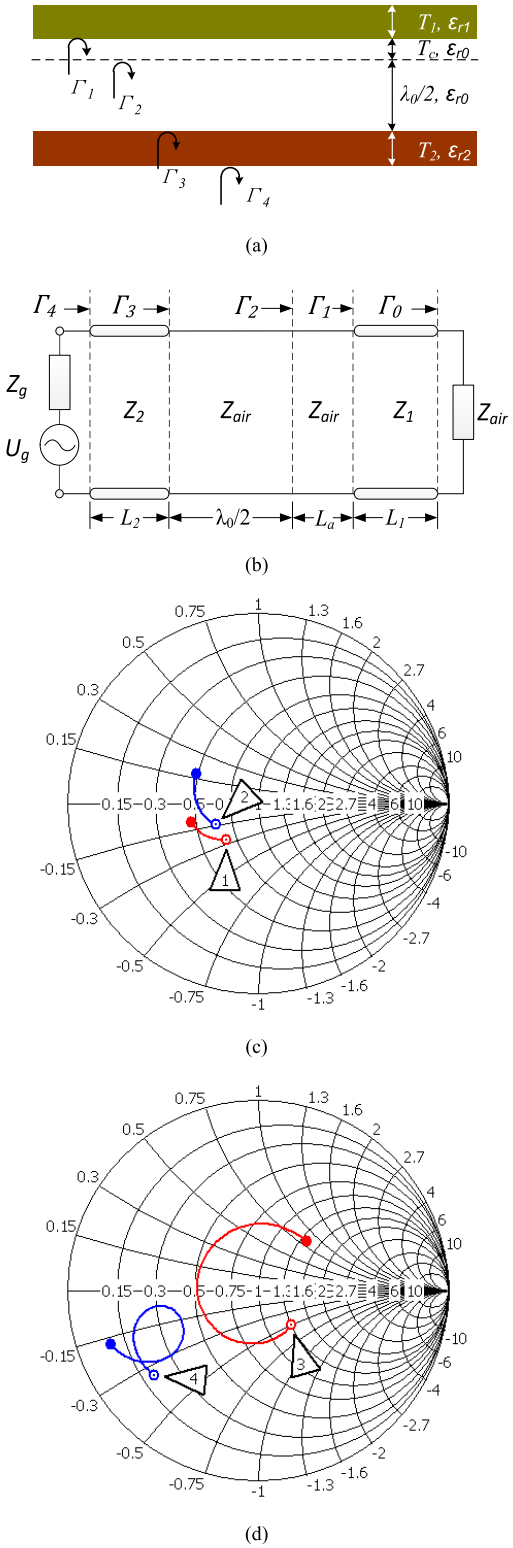

FIGURE 4. Equivalent circuit analysis: (a) superstrate structure, (b) equivalent circuit, (c) and (d) analysis on Smith Chart normalized to Z_{air} (○: $f_0-\delta f$, ●: $f_0+\delta f$).

in Fig. 4d. The swirled part produces a positive reflection phase slope in the vicinity of f_0. It is worth noting that if $0 \le \varphi_1 \le \pi$, namely $\lambda_d/2 \ge T_1 \ge \lambda_d/4$, we will have

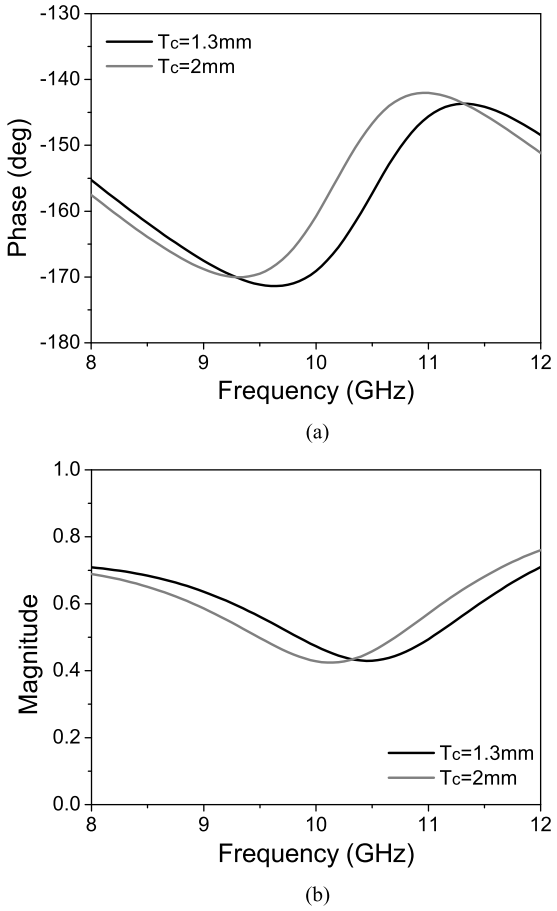

FIGURE 5. Reflection phase and magnitude of the superstrate structure with different values of T_c.

$T_c \leq 0$ and $T_c+\lambda_0/2 \leq \lambda_0/2$. For that case the design method remains applicable.

Again, we select Rogers RT/duroid 5880 ($\varepsilon_{r1} = 2.2$) with thickness $T_1 = 3.175$ mm and Rogers RT/duroid 6006 ($\varepsilon_{r2} = 6.15$) with thickness $T_2 = 1.9$ mm to construct the full-dielectric superstrate structure working in X band. Their thicknesses are both around $\lambda_d/6$ at 10 GHz. Fig. 5 shows the reflection phase and magnitude with different values of T_c. It is found that reflection phase with a positive slope is obtained which is similar to that in Fig. 3, and T_c affects the resonance frequency. At present, wideband FPRAs can be designed with electrically thin dielectric substrates based on the above analysis. However, two kinds of substrates with different permittivities are still indispensable.

The air layer T_c does not affect the magnitude of Γ_1, and therefore we have $|\Gamma_2| = |\Gamma_1|$. Further, the top dielectric superstrate with the air layer T_c can be equivalent to a substrate layer with thickness $\lambda_d/4$ at f_0 and permittivity ε_{re1}. According to the transmission line theory, ε_{re1} can be formulated as

$$\varepsilon_{re1} = \frac{1+|\Gamma_{1\_0}|}{1-|\Gamma_{1\_0}|} \tag{4}$$

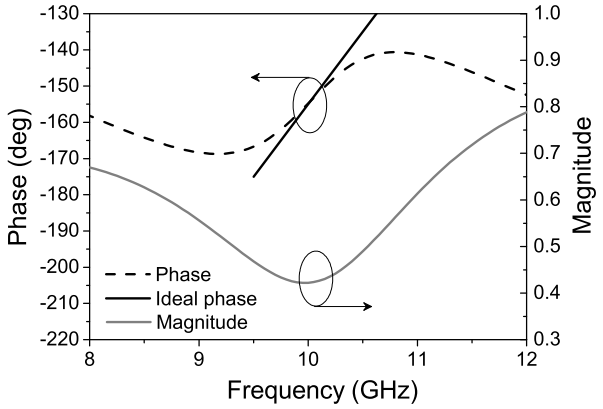

FIGURE 6. Reflection phase and magnitude of the superstrate structure.

where Γ_{1_0} is the reflection coefficient Γ_1 at f_0. Likewise, similar equivalence can also be made for the bottom dielectric superstrate with $\lambda_d/4$ at f_0 and ε_{re2}. As mentioned earlier, one of the necessary conditions for the structure in Fig. 2a producing reflection phase proportional to frequency is $\varepsilon_{r2} > \varepsilon_{r1}$ [10]. For the case shown in Fig. 4a, $\varepsilon_{r2} > \varepsilon_{r1}$ is replaced with $\varepsilon_{re2} > \varepsilon_{re1}$ to make the condition $\varepsilon_{r2} > \varepsilon_{r1}$ not decisive. In other words, two dielectric substrate layers with $\varepsilon_{r2} \leq \varepsilon_{r1}$ can also be used to construct the superstrate structure with reflection phase proportional to frequency, consequently making FPRA designs cost-effective and flexible. Likewise, a larger value of $\varepsilon_{re2}/\varepsilon_{re1}$ can produce a higher gain, but will diminish the gain bandwidth.

As an example, Rogers RT/duroid 6006 ($\varepsilon_{r1} = \varepsilon_{r2} = 6.15$) with thickness $T_1 = 0.635$ mm and $T_2 = 1.9$ mm are selected to construct the full-dielectric superstrate structure working in X band. Their thicknesses are around $\lambda_d/19$ and $\lambda_d/6$ at 10 GHz, respectively. Fig. 6 shows the reflection phase and magnitude while $T_c = 2.7$mm. The reflection phase is proportional to frequency in the range of 9.2-10.8 GHz with $|\Gamma_4| \geq 0.43$. This superstrate structure will be applied to a wideband FPRA design next.

III. FEED ANTENNA DESIGN

The feed antenna, working as the exciting source of an FPRA, also plays an important role on the performance. As reported in the literature, several kinds of radiators have been used as feed antennas for FPRAs, such as a waveguide aperture [12], a probe-fed patch antenna [13], a metal strip suspended over the ground plane [14], and even a patch array [15]. A patch antenna is a good candidate with its advantages including a low profile, ease of feeding and potential of wideband operation. An air gap loaded slot coupled patch antenna is designed and optimized as the feed for the wideband FPRA to be designed. The configuration is shown in Fig. 7.

Commercial laminate Rogers RT/duroid 5880 ($\varepsilon_r = 2.2$, $\tan\delta = 0.0009$) with thickness 0.787 mm is used in the design. The parasitic patch is coupled with the feed line through a slot in the ground plane. The patch and ground plane are spaced by an air gap to suppress surface wave which

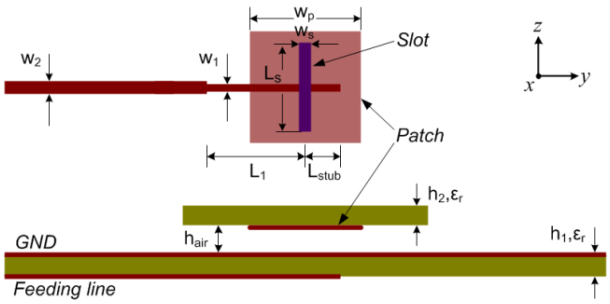

FIGURE 7. Configuration of the slot-coupled patch antenna used to feed the wideband FPRA.

TABLE 1. Dimensions of the patch antenna.

Parameter	Value/mm	Parameter	Value/mm
W_p	9.2	L_{stub}	3
W_1	1.2	L_1	9.5
W_2	2.3	h_1	0.787
W_s	1	h_2	0.787
L_s	8	h_{air}	2.5

can be introduced to the cavity and degrades performance of the FPRA [16]. A compact matching network is added to the feed line to enhance the impedance bandwidth. Dimensions of the antenna are listed in Table I.

Simulated reflection coefficient (S_{11}) and radiation gain of the patch antenna are plotted in Fig. 8 and Fig. 9, respectively. The impedance bandwidth covers a frequency band from 9 GHz to 11.2 GHz for S_{11} less than -10 dB. Within this band, the radiation gain increases with frequency, ranging from 5.8 dBi to 8.5 dBi. The performance of this patch antenna is expected and satisfactory.

IV. WIDEBAND FPRA DESIGN

The wideband FPRA to be designed is a combination of the superstrate structure and feed antenna. According to the FPRA configuration shown in Fig. 1, there are still two parameters W and h_{c2} not determined.

Assuming the lateral size W infinite, the directivity of the FPRA relative to that of the feed antenna can be formulated as [8],

$$D_r = 10 \log \left(\frac{1+\Gamma}{1-\Gamma} \right) \tag{5}$$

where D_r is the relative directivity, and Γ is the reflection magnitude of the superstrate structure. Because the FPRA is fed at the center of the cavity, a tapered field behaving like a Gaussian distribution along the lateral direction is obtained. For a required directivity, the antenna size can be estimated by [17],

$$S = \frac{10^{D/10} \cdot \lambda^2}{0.8\pi^2} \tag{6}$$

where S is the antenna surface area, λ is the free space wavelength. At 10 GHz, the directivity of the feed antenna is

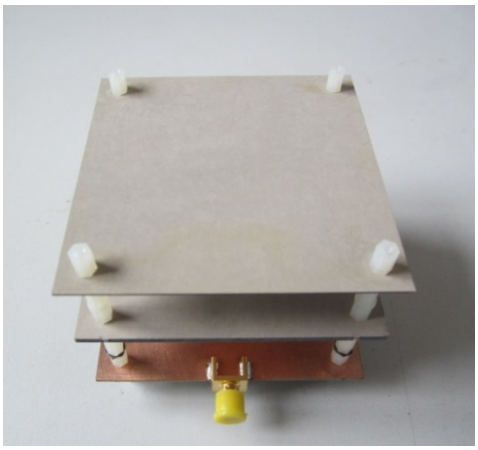

FIGURE 8. Prototype of the wideband FPRA structure.

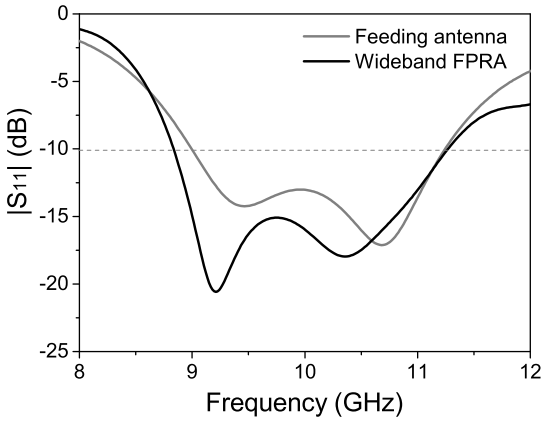

FIGURE 9. Simulated $|S_{11}|$ of the feed antenna and the wideband FPRA.

around 8 dBi, and the reflection magnitude of the superstrate structure is $\Gamma = 0.43$. Directivity of the FPRA at 10 GHz is expected to be $D = (8 + D_r)$ dBi ≈12 dBi. Considering that wideband operation is pursued, a slightly larger aperture size W should be specified. A preliminary determination of h_{c2} can be made with the aid of Formula (1), and further optimization need to be performed by full wave simulation.

The side view of the wideband FPRA is shown in Fig. 1. It is modeled and simulated by using the commercial EM software CST Microwave Studio. All the air gaps are created with hexagonal nylon spacers with diameter of 2.3 mm at each four corners, and they are taken into account during simulation. The resonance condition for the FPRA, namely Formula (1), is formulated based on the analysis of plane wave excitation. That is different from the actual situation of using a feed antenna in the cavity as the source, and therefore W, h_{c1} and h_{c2} are further optimized. Finally, they are set as $W = 72$ mm, $h_{c1} = 20.3$ mm and $h_{c2} = 17$ mm.

Simulated reflection coefficient of the wideband FPRA is plotted in Fig. 9. Compared with the feed antenna, the impedance band extends to lower frequency. Fig. 10 plots simulated gain of the feed antenna, the wideband FPRA, and

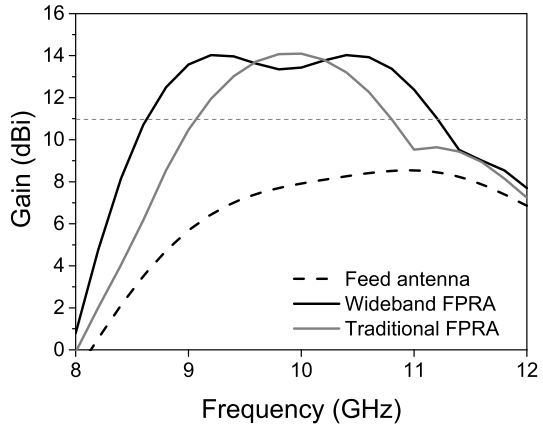

FIGURE 10. Simulated gain of the feed antenna, the wideband FPRA and a conventional FPRA.

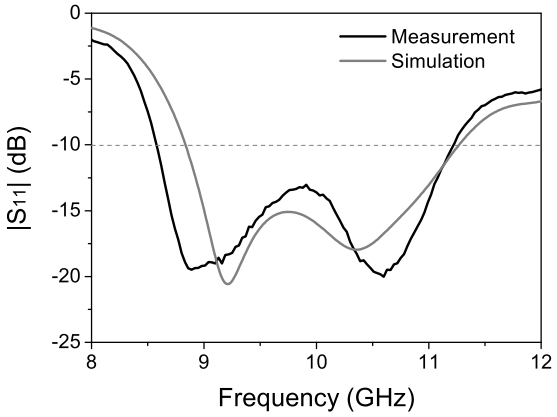

FIGURE 11. Simulated and measured $|S_{11}|$ of the wideband FPRA.

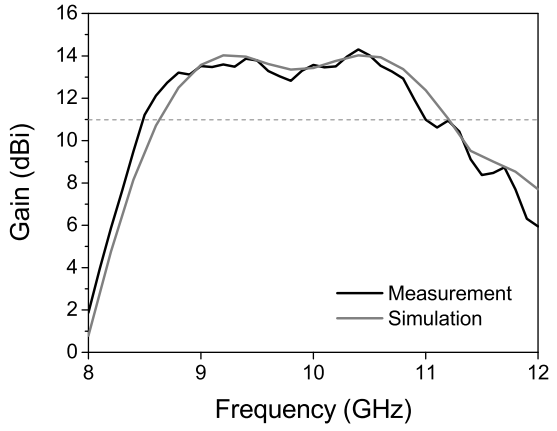

FIGURE 12. Simulated and measured gain of the wideband FPRA.

a conventional FPRA achieving the same peak gain. The gain of the feed antenna has been significantly enhanced. The 3 dB gain bandwidth of the wideband FPRA is wider than that of the conventional one.

With the dimensions determined already, a prototype is fabricated and assembled, as shown in Fig. 8. A 50 Ohm SMA connector is soldered to the antenna as the feed port.

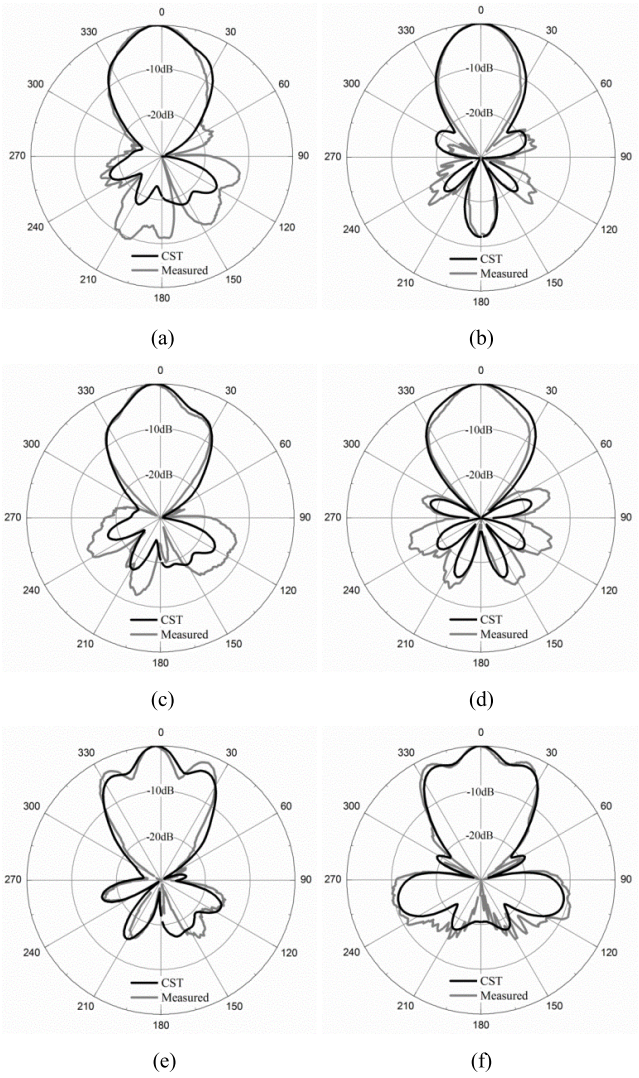

FIGURE 13. Radiation patterns: (a) E-plane at 9 GHz, (b) H-plane at 9 GHz, (c) E-plane at 10 GHz, (d) H-plane at 10 GHz, (e) E-plane at 11 GHz, and (f) H-plane at 11 GHz.

Reflection coefficient, radiation patterns and gain are measured in a microwave anechoic chamber to validate the design and analysis.

Measured and simulated reflection coefficients are plotted in Fig. 11. The measured impedance bandwidth of the wideband FPRA for $S_{11} \leqslant -10$ dB ranges from 8.5 GHz to 11.2 GHz, relatively 27%, whereas the simulated bandwidth ranges from 8.8 GHz to 11.3 GHz, relatively 25%. Discrepancies between the two results are probably caused by assembly and SMA connector soldering tolerances.

Measured and simulated gains are plotted in Fig. 12, and they agree well with each other. The 3 dB gain bandwidth of the wideband FPRA is from 8.6 GHz to 11.2 GHz, relatively 27%, with a peak gain of 14 dBi. Besides, the 3 dB gain band is coincident with the impedance band. It is worth noting that a conventional FPRA can only provide a gain bandwidth of 17% with the same peak gain.

Measured and simulated E-plane (*yoz*) and H-plane (*xoz*) radiation patterns at 9 GHz, 10 GHz and 11 GHz are plotted in Fig. 13. The wideband FPRA produces directive radiation in both E-plane and H-plane with peak radiations occurring at broadside and sidelobes less than −15 dB. The high radiation levels at backside are caused by backward radiation of the feed antenna and the SMA connector. Polarization characteristic of the wideband FPRA is coincident with that of the feed antenna. Furthermore, dual-polarized or circularly polarized FPRAs can be obtained by using dual polarized or circularly polarized feed antennas.

V. CONCLUSION

A detailed design method of wideband FPRAs with two layers of full-dielectric superstrates is presented. The dielectric superstrates are allowed to have the same or different permittivities, and are not necessary to be with a fixed electrical thickness when working frequency is specified. These features improve the cost performance and the design flexibility effectively. The reflection phase of the superstrate structure increases with frequency and approximately satisfies the resonance condition with in a wide frequency band. A wideband FPRA working in X band is designed as an example using the proposed method, whereafter experiments are carried out, having the method validated.

Finally, in order to facilitate the application of the proposed method, the design process is briefly concluded as the following nine steps:

1) Select two kinds of dielectric substrates with different electrical thicknesses T ($T < \lambda_d/2$) or different permittivities ε_r.

2) Calculate the reflection magnitude and phase of the substrates with plane wave excitation by commercial EM softwares or the transmission line theory.

3) Calculate equivalent permittivities of both dielectric substrates using Formula (4). The substrate with the lower equivalent permittivity serves as the top superstrate.

4) Calculate the air layer thickness T_c using Formula (3), the value of which could be positive or negative.

5) Calculate the reflection magnitude and phase of the superstrate structure composed of the two dielectric slabs spaced by $h_{c1} = T_c + \lambda_0/2$.

6) Calculate the cavity height h_{c2} between the superstrate structure and the ground plane.

7) Design a wideband antenna suitable for being as the feed of the wideband FPRA to be designed.

8) Estimate the dimension of the wideband FPRA using Formula (5), Formula (6) and the gain of the feed antenna. Empirically a larger size should be selected.

9) Model the wideband FPRA using commercial EM softwares. Optimize the antenna by full-wave simulation and determine all the parameters including h_{c1}, h_{c2} and W.

REFERENCES

[1] R. Orr, G. Goussetis, and V. Fusco, "Design method for circularly polarized Fabry-Perot cavity antennas," *IEEE Trans. Antennas Propag.*, vol. 62, no. 1, pp. 19–26, Jan. 2014.
[2] G. V. Trentini, "Partially reflecting sheet arrays," *IEEE Trans. Antennas Propag.*, vol. AP-4, no. 4, pp. 666–671, Oct. 1956.
[3] Z.-G. Liu, Z.-X. Cao, and L.-N. Wu, "Low-profile circularly polarized Fabry-Perot resonator antenna fed by linearly polarized microstrip patch," *IEEE Antenna Wireless Propag. Lett.*, vol. 15, pp. 524–527, 2016.
[4] B. A. Zeb, N. Nikolic, and K. P. Esselle, "A high-gain dual-band EBG resonator antenna with circular polarization," *IEEE Antenna Wireless Propag. Lett.*, vol. 14, pp. 108–111, 2015.
[5] F. Qin *et al.*, "A triband low-profile high-gain planar antenna using Fabry-Perot cavity," *IEEE Trans. Antennas Propag.*, vol. 65, no. 5, pp. 2683–2688, May 2017.
[6] N. Wang, Q. Liu, C. Wu, L. Talbi, Q. Zeng, and J. Xu, "Wideband Fabry-Perot resonator antenna with two complementary FSS layers," *IEEE Trans. Antennas Propag.*, vol. 62, no. 5, pp. 2463–2471, May 2014.
[7] F. Sultan and S. S. I. Mitu, "Superstrate-based beam scanning of a Fabry-Perot cavity antenna," *IEEE Antenna Wireless Propag. Lett.*, vol. 15, pp. 1187–1190, 2016.
[8] N. Wang, C. Zhang, Q. Zeng, N. Q. Wang, and J. Xu, "New dielectric 1-D EBG structure for the design of wideband resonator antennas," *Progr. Electromagn. Res.*, vol. 141, pp. 233–248, 2013.
[9] L. Leger, T. Monediere, and B. Jecko, "Enhancement of gain and radiation bandwidth for a planar 1-D EBG antenna," *IEEE Microw. Wireless Compon. Lett.*, vol. 15, no. 9, pp. 573–575, Sep. 2005.
[10] N. Wang, J. Li, G. Wei, L. Talbi, Q. Zeng, and J. Xu, "Wideband Fabry-Perot resonator antenna with two layers of dielectric superstrates," *IEEE Antenna Wireless Propag. Lett.*, vol. 14, pp. 229–232, 2015.
[11] M. A. Al-Tarifi, D. E. Anagnostou, A. K. Amert, and K. W. Whites, "Bandwidth enhancement of the resonant cavity antenna by using two dielectric superstrates," *IEEE Trans. Antennas Propag.*, vol. 61, no. 4, pp. 1898–1908, Apr. 2013.
[12] A. P. Feresidis and J. C. Vardaxoglou, "A broadband high-gain resonant cavity antenna with single feed," in *Proc. EuCA*, Nice, France, Nov. 2006, pp. 1–5.
[13] L. Moustafa and B. Jecko, "Design and realization of a wide-band EBG antenna based on FSS and operating in the ku-band," *Int. J. Antennas Propag.*, vol. 2010, Mar. 2010, Art. no. 139069.
[14] Y. Ge, K. P. Esselle, and T. S. Bird, "The use of simple thin partially reflective surfaces with positive reflection phase gradients to design wideband, low-profile EBG resonator antennas," *IEEE Trans. Antennas Propag.*, vol. 60, no. 2, pp. 743–750, Feb. 2012.
[15] A. R. Vaidya, R. K. Gupta, S. K. Mishra, and J. Mukherjee, "High-gain low side lobe level fabry perot cavity antenna with feed patch array," *Progr. Electromagn. Res. C*, vol. 28, pp. 222–238, 2012.
[16] R. Garg, P. Bhartia, I. Bahl, and A. Ittipiboon, *Microstrip Antenna Design Handbook*. Norwood, MA, USA: Artech House, 2001, ch. 1, pp. 43–47.
[17] L. Leger, C. Serier, R. Chantalat, M. Thevenot, T. Monediere, and B. Jecko, "1D dielectric electromagnetic band gap (EBG) resonator antenna design," *Ann. Télécommun.*, vol. 59, nos. 3–4, pp. 242–260, 2004.

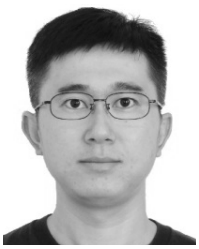

NAIZHI WANG received the M.S. and Ph.D. degrees in electronic science and technology from Northwestern Polytechnical University, Xi'an, China, in 2012 and 2014, respectively. He is currently a Senior Engineer with the 14th Research Institute of China Electronics Technology Group Corporation, Nanjing, China.

During 2011 to 2013, he was sponsored by the China Scholarship Council as a Visiting Student with the University of Quebec in Outaouais, Gatineau, QC, Canada, and contributed in the design, integration, and testing of millimeter-wave antennas. His current research interests include designs and applications of millimeter-wave antennas, frequency selective surfaces, and wideband active phased array antennas.

LARBI TALBI (S'95–M'97–SM'05) received the M.S. and Ph.D. degrees in electrical engineering from Laval University, Quebec City, QC, Canada, in 1989 and 1994, respectively. From 1994 to 1995, he was a Post-Doctoral Fellow with the Per sonal Communications Research Group, INRS-Telecommunications, Montreal, QC, Canada, where he led projects supported by Bell Canada. From 1995 to 1998, he was an Assistant Professor with the Electronics Engineering Department, Riyadh College of Technology, Saudi Arabia. During 1998–1999, he was an Invited Professor with the Electrical and Computer Engineering Department, Laval University. In 1999, he joined the Department of Computer Science and Engineering (DCSE), University of Quebec in Outaouais (UQO), Gatineau, QC, Canada, as a Professor. In 2005, he spent his sabbatical leav e as an Invited Researcher with the Communication Research Center, Ottawa, ON, Canada, within the Propagation Research (RVEP) Group, Satellite Communications and Radio Propagation Branch (VPSAT). In 2006, he joined the Electrical and Electronics Engineering Department, Dumlupinar University, Turkey, as a Visiting Professor. From 2007 to 2013, he was the Ph.D. Program Chair in sciences and information technologies and the Chair of the department from 2013 to 2015. He has a very strong collaboration with the Telebec Wireless Underground Communication Laboratory, Val-d'Or, QC, Canada. He is currently a Full Professor with the DCSE, UQO. He has authored or co-authored over 200 journal and conference technical papers. His research activities include experimental characterization and modeling of UHF/extremely high frequency indoor radio propagation channels and design of antennas and microwave circuits for wireless communication systems. He is currently actively involved in major projects related to the deployment of wireless technologies in underground mines, mainly, the experimental characterization of the underground mine channels using multi-in multi-out antennas at 60 GHz, the design of microwave and RF components using substrate integrated waveguide technique, transparent antennas, metamaterials applied to microwave design, and antenna array for wireless applications. He received the Best Paper Prize from the IET—ICWCA Conference, Malaysia, in 2013.

Dr. Talbi is a member of the Order of Engineers of Quebec. He frequently serves as a technical program committee member for international and national conferences. He is an Associate Editor of the *International Journal of Antennas and Propagation* (Hindawi Publishing Corporation). He regularly acts as a reviewer for many international scientific journals and conferences and also for research funding organizations.

QINGSHENG ZENG (SM'11) received the Ph.D. degree from the University of Ottawa, Canada. He has been a Research Engineer and a Senior Research Engineer with the Communications Research Centre Canada, Government of Canada. He is currently a Distinguished Professor and a Ph.D. Advisor with the Nanjing University of Aeronautics and Astronautics, an Adjunct Professor and a Ph.D. Advisor with the University of Ottawa, Carleton University, Université du Québec an Outaouais, and the Institut National de la Recherche Scientifique-Centre Energie, Matériaux et Télécommunications, and a Guest Professor with Harbin Engineering University, Northwestern Polytechnic University, the Beijing University of Post and Telecommunications, and Beijing Jiaotong University. He has undertaken research and teaching in several fields, including antenna analysis and design, electromagnetic compatibility (EMC) and electromagnetic interference, ultra wideband technology, radio wave propagation, computational electromagnetics.

He has been a member of the Strategic Projects Grant (Selection Panel (Information and Communications Technologies B) for the Natural Sciences and Engineering Research Council of Canada (NSERC), a member of Site Visit Committee of NSERC Industrial Research Chair, and a Reviewer of the NSERC Industrial R&D Fellowships. He is a member of the IEEE Canada Industry Relations Committee. He is the Chair of the Antennas and Propagation/Microwave Theory and Techniques Joint Chapter and a Secretary of the EMC Chapter of the IEEE Ottawa.

He has published over 100 SCI and EI indexed papers and technical reports. He has authored one book and co-authored two book chapters, one of which has been downloaded over 3000 times only in one year after it was published in 2011. He received several technical and technical service awards, was ranked as one of the researchers at Communications Research Centre Canada with the strongest impacts in 2011, and selected as a Distinguished Expert under the Plan of Hundreds of Talents of Shanxi Province, China, in 2015, and an Oversea Prestigious Advisor of Guangdong Province in 2017. He has been serving as an editorial board member and a reviewer for a number of technical books and scientific journals, as the conference co-chair, a session organizer and chair, a technical program committee member, a reviewer, a short course/workshop/tutorial presenter, and a keynote speaker for many international and national symposia.

JIADONG XU was born in Nanjing, China, in 1948. He received the M.S. degree from Northwestern Polytechnical University, Xi'an, China, in 1981.

He has over 40 years of research experience in the field of RF designs, microwave measurements, and electromagnetic computation. Since 1990, he has been a Full Professor with the School of Electronics and Information, Northwestern Polytechnical University. He has authored over 200 academic journal and conference papers and led numerous projects from the government and industry. He received several national awards.